Case Studies in Construction Materials 24 (2026) e05784

Contents lists available at ScienceDirect

Case Studies in Construction Materials

journal homepage: www.elsevier.com/locate/cscm

Thermal decomposition in blended cement systems and its effect on fire-induced concrete spalling: Insights from XRD and TGA

Tim Pittrich [a,*], Daniel Jansen [b], Frank Weise [a], Ludwig Stelzner [a], Frank Dehn [c]

[a] Federal Institute for Materials Research and Testing, Unter den Eichen 87, Berlin 12205, Germany
[b] University of Erlangen-Nuremberg, Schloßgarten 5a, Erlangen 91054, Germany
[c] Karlsruhe Institute of Technology, Gotthard, Franz Straße 3, Karlsruhe 76131, Germany

ARTICLE INFO

Keywords:
Fire concrete spalling
High temperatures
Blended cements
Dehydration
XRD
TGA

ABSTRACT

Blended cements are gaining increasing popularity due to their lower CO_2-footprint in comparison to ordinary Portland cement (OPC). However, this growing use raises the potential risk of buildings made with blended cement concrete being exposed to fire, which can lead to heavy damages caused by explosive concrete spalling. It has already been shown that the cement type strongly influences the fire-induced concrete spalling and the thermally induced moisture transport, however, to understand the mechanisms behind these findings the thermal decomposition behavior of the cementitious matrix must be investigated more systematically. Therefore, the phase content of three blended cement pastes (CEM II/A-LL, CEM III/A and CEM II/B-Q) was studied in comparison with a Portland cement paste (CEM I) after temperature exposure to 20 °C, 105 °C, 300 °C and 500 °C. Clear differences in the initial phase composition and their dehydration behavior between the individual cement types were recognized. In conclusion, blended cements showed lower amounts of AFt and AFm phases and additionally lower amounts of portlandite and C-(A)-S-H were found in CEM III/A and CEM II/B-Q pastes. The results suggest that higher AFt and AFm contents in CEM I, which are associated with greater water release at relatively low temperatures may ultimately reduce the spalling risk. Furthermore, C-(A)-S-H in CEM III/A and CEM II/B-Q showed increased thermal stability and large amounts of non-hydrated phases were found in every blended cement paste. Both of those aspects might contribute to thermomechanical spalling and the overall increased spalling susceptibility observed in blended cement concrete.

1. Introduction

Nowadays, blended cements gain attention as their utilization is an effective way to reduce the CO_2-emssions caused by the ordinary Portland cement (OPC) production. In blended cements part of the Portland cement clinker is replaced by fillers and/or supplementary cementitious material (SCM). These materials can be of natural origin (e.g. limestone) or man-made materials such as by products from the steel or power industry. Therefore, there is a wide range of usable materials that influence concrete properties on the mineralogical level. The mineralogical composition of non-hydrated and hydrated OPC and blended cements is already well known.

* Corresponding author.
E-mail addresses: tim.pittrich@bam.de (T. Pittrich), daniel.jansen@fau.de (D. Jansen), frank.weise@bam.de (F. Weise), ludwig.stelzner@bam.de (L. Stelzner), frank.dehn@kit.edu (F. Dehn).

https://doi.org/10.1016/j.cscm.2026.e05784
Received 17 October 2025; Received in revised form 12 December 2025; Accepted 8 January 2026
Available online 13 January 2026

OPC mainly consists of the clinker phases C_3S, C_2S, C_3A and C_4AF[1] and minor amounts of free lime (CaO). In addition, it contains sulfate carriers in the form of gypsum, anhydrite or bassanite as well as secondary components such as limestone. Blended cements contain the same clinker minerals but fillers and/or SCMs are used to replace fractions of the Portland cement clinker. Up to now most commonly used fillers and SCMs are limestone (LS), fly ash (FA) and blast furnace slag (BFS). However, the long-term availability of FA and BFS is questionable and therefore the interest in alternatives such as calcined clays (CC) rise as their raw material is globally available and they provide good pozzolanic properties after activation [1]. During hydration clinker minerals mainly form C-S-H and portlandite as well as sulfoaluminate phases in the form of ettringite (AFt) which in later hydration stages partly converts into AFm phases. In addition to the regular hydration process blended cements experience further pozzolanic or latent hydraulic reactions. The pozzolanic reaction describes the consumption of portlandite during the presence of water and a reactive silicate bearing SCM leading to the formation of additional C-S-H or C-(A)-S-H respectively. Therefore, blended cements in general show lower amounts of portlandite [2].

Due to the increasing popularity of blended cements the probability of buildings made with blended cement concrete being exposed to fire rises. When exposed to fire, concrete undergoes various chemical and physical changes, which cause an overall decrease in strength and in the worst-case explosive spalling. Responsible for spalling are thermohydraulic and thermomechanical mechanisms. While neither is yet fully understood, several contributing factors have been identified. The thermohydraulic spalling mechanism is often associated with an increase in pore pressure and/or the sudden evaporation of superheated water within the concrete matrix. These processes generate internal stresses that can exceed the tensile strength of the material, leading to explosive spalling. The thermomechanical mechanisms are linked to restrained thermal expansion and thermal incompatibility between cement paste and the aggregates. These mismatches can induce significant internal stresses, which may also result in spalling. A comprehensive overview of various theories and mechanisms related to concrete spalling can be found in [3]. Many studies showed that the cement type used influences fire induced concrete spalling, however, the reasons behind those findings remain rather unclear [4]. During a fire event, it can be assumed that the point of time and amount of water release, which depends heavily on the dehydration of the different mineral phases found in different types of hardened cement paste, has a decisive influence on thermohydraulic processes. Of particular interest is the temperature range between 250 °C and 450 °C, as fire-induced spalling typically occurs within this range. To understand those differences, further understanding of the decomposition of blended cement pastes at elevated temperatures is necessary. The general dehydration and decomposition behavior of hardened cement paste can be described as follows (Fig. 1): Initially, free and physical bound water within the capillary pores begins to evaporate at temperatures up to approximately 200 °C. Between 80 and 150 °C, ettringite starts to dehydrate accompanied by the gradual loss of chemically bound water from the C-S-H, which ultimately decomposes into β-C_2S between 600 and 800 °C. The AFm phases release their water in the range of 130–180 °C. Portlandite ($Ca(OH)_2$) dehydrates between 460 and 540 °C, forming CaO. From around 600 °C, calcium carbonate ($CaCO_3$) also begins to decompose into CO_2 and CaO [5,6].

Even though the basic principle of thermal decomposition remains very similar in all cementitious systems, there can be significant differences in water release and decomposition of the cement matrix depending on the phase type and content. Investigations by Zhang and Ye [7] as well as Saillio et al. [8] looked at the quantitative phase development of OPC cement paste exposed to elevated temperatures. Zhang and Ye analyzed hardened Portland cement paste with a water to cement ratio (w/c) of 0.5 cured for 28 d by X-ray diffraction (XRD) with subsequent Rietveld analysis. In total, the samples were exposed to ten different temperatures starting at 105 °C up to 1000 °C. It was observed that the phase composition barely changes between 105 and 400 °C. At 500 °C, the crystallinity decreases and the dehydration of portlandite was noticed accompanied with the formation of amorphous lime. At temperatures above 600 °C the crystallinity increased again which was caused by the decomposition of amorphous C-S-H into β-C_2S. In addition, the formed lime started to become more and more crystalline with higher applied temperatures. It should be noted that the content of all amorphous phases was summarized in this study and therefore no precise information concerning the amounts of C-S-H, ettringite, AFm etc. was given. The group of Saillio et al. [8] took a closer look into the phase assemblage of a 5-year-old Portland cement paste submitted to various high temperature and cooling regimes, including air and water quenching. The pastes, prepared with a w/c of 0.272, were subjected to temperatures between 100 °C and 1000 °C. Subsequently, the samples were subjected to either air cooling or water quenching in a freshwater tank, simulating the thermal shock that may occur during real-life fire extinguishing scenarios. The quantification of the phase assemblage before and after heating was conducted by a method combining XRD, nuclear magnetic resonance (NMR) spectroscopy, inductively coupled plasma atomic emission spectroscopy (ICP-AES) and thermal gravimetric analysis (TGA) stated in [9]. Due to the allowance of air- and water-cooling rehydration happened which led to the presence of hydrated phases also after heating especially in the water-cooled samples. Standing out was once again the dehydration of portlandite at 500 °C as well as the gradual decomposition of C-S-H which finally resulted in the formation of anhydrous phases mostly C_2S and C_3S. Research conducted by Song et al. [6] analyzed the phase transformation of Portland cement blended with slag qualitatively by means of High-Temperature X-ray diffraction (HT-XRD). The OPC reference and the OPC-BFS (74 wt% BFS, 6 wt% gypsum) were made with a water to binder ratio of 0.4 and cured for 3 d, 28 d and 56 d. Upon the respective day of testing, the samples were placed in the diffractometer and simultaneously heated with 1 K/min until the specific temperature was reached. Finally, the XRD patterns were recorded. Next to the composition differences caused by the raw materials, slight differences of the mineral phase composition in the initial state appeared. Minor traces of hydro garnet were only found in the hardened OPC paste as well as much lower contents of portlandite in the OPC-GBFS sample. After exposure to high temperatures the first phase to decompose was ettringite at 75 °C followed

[1] Cement chemistry notation will be used in this paper: C = CaO; S = SiO_2; A = Al_2O_3; F = Fe_2O_3; $ = SO_3; H = H_2O

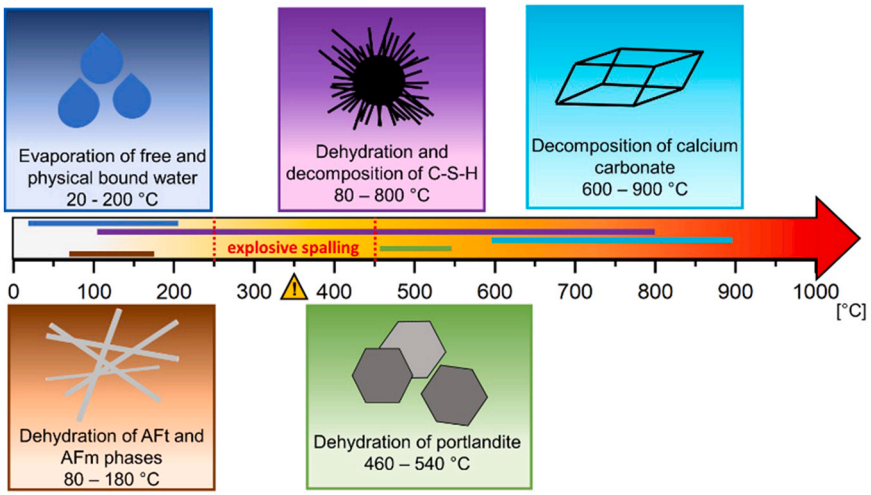

Fig. 1. Schematic representation of the dehydration and decomposition of the main phases in hardened cement paste in concrete.

by the AFm phases which disappeared at 160 °C in both pastes. Thereupon, hydrogarnet decomposed between 200 and 380 °C in the hardened OPC paste. The decomposition of the main binder phase C-S-H was firstly noted after exposure to 400 °C where the CaO layers got destroyed. However, the actual dehydration already starts at temperatures around 80 °C. This early stage of dehydration is not detectable in XRD patterns, as moderate temperatures primarily affect the interlayer spacing of hydration products without altering their crystalline structure. Beyond 600 °C the dehydration of portlandite and decomposition of CaO_3 was reported. Furthermore, the formation of α_1-C_2S, and lime was observed during the high temperature exposure. Lin et al. [10] studied the thermal decomposition behavior of OPC, as well as binary and ternary blends of OPC with LS and CC after 180 d of curing, over a temperature range of 20 – 900 °C. Key findings included the formation of monocarboaluminate in limestone-containing blends, and both monocarboaluminate and hemicarboaluminate in limestone calcined clay cement (LC^3) systems. The peak intensity increased with higher proportions of limestone and calcined clay. Upon exposure to 300 °C, the AFt and AFm phases were no longer detectable. Instead, katoite was observed, which was reported to positively influence strength development. At higher temperatures of 550 °C, katoite and portlandite decomposed and a further increase up to 900 °C led to the decomposition of calcium carbonate and eventually C-S-H. Cao et al. [11] investigated the thermal stability of LC^3 between 100 and 400 °C. An OPC reference mix was compared to a LC^3 mix consisting of 53 wt.-% OPC, 30 wt.-% CC 15 wt.-% LS and 2 wt.-% gypsum prepared with a w/b of 0.325. The samples were measured after 150 d of hydration. Due to the use of calcined clay and limestone, significant quartz and calcite peaks were present. After exposure to 50 °C, both ettringite and monocarboaluminate were still present in the two pastes. However, it was stated that due to the synergetic reaction between CC, LS and portlandite increased contents of monocarboaluminate phases were detected in LC^3 samples. Further temperature increases up to 100 °C led to the decomposition of ettringite and a partial conversion of monocarboaluminate into hemicarboaluminate. Both AFm type phases dehydrated and disappeared completely at 200 °C. The pattern's crystallinity between 2θ angles of 25 – 35 ° decreased which was attributed to the dehydroxylation of the C-(A)-S-H. Lower amounts of portlandite were recorded in the LC^3 specimens due to its pozzolanic character, the total amount in both mixes decreased noticeably at 400 °C. Additionally, the phases katoite and strätlingite formed after an exposure to 100 °C. Studies by Donatello et al. [12] analyzed the phase evolution of a high-volume FA blended cement paste in comparison to a Portland-composite cement CEM II/A-M paste with a w/b of 0.32 and 0.36, respectively, after 70 d of curing. In the initial state due to the large amount of pozzolans, the high-volume FA paste showed no portlandite. In addition, C-S-H was recorded as well as the typical FA phases quartz, anorthite, maghemite and hematite. After 800 °C, the appearance of laihunite was noted. The CEM II/A-M sample showed the typical hydration phases of a cementitious binder in the form of C-S-H, portlandite and ettringite. Based on the raw material's composition, calcite and slag could also be

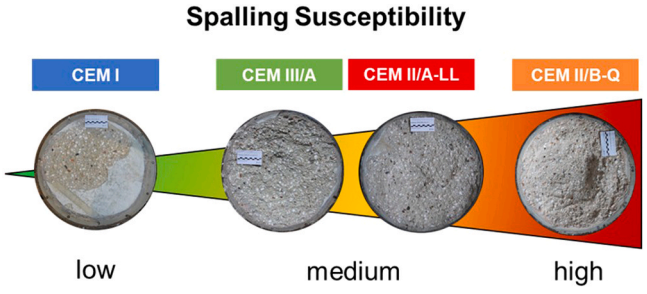

Fig. 2. Spalling susceptibility of normal strength concrete with different types of cement after HC fire exposure.

identified.

Although numerous studies have investigated the thermal decomposition and dehydration behavior of cementitious materials [13–15], their impact on concrete's spalling behavior has often been overlooked. However, with the growing adoption of low-carbon blended cements in sustainable construction, interest in understanding the spalling behavior of blended cement concrete has increased significantly in recent years [4]. In-depth spalling studies on concretes with standardized blended cements, such as, CEM II/A-L(L), CEM II/B-V, and CEM III/A, conducted by various research groups have produced both consistent findings but also contradictions [16–19]. However, phase assemblage and phase transformations at high temperatures, which strongly influence concrete properties, have never been included in these investigations. In our previous research we showed that blended cements increase the spalling susceptibility of normal strength concrete used for tunnel construction when exposed to hydrocarbon (HC) fire (Fig. 2) [20]. We also demonstrated that the cement type significantly influences the thermally induced moisture transport during one-sided heating [21]. As mentioned above, there is only very limited information available on the quantitative phase transformation of blended cement pastes due to high-temperature exposure with regards to explosive spalling, in particular for cement mixes containing calcined clays. Especially the type and number of hydrated phases with their corresponding dehydration behavior are of interest to evaluate their impact on thermohydraulic effects. Thus, in-depth studies were carried out regarding the phase development in four different cement pastes (CEM I, CEM II/A-LL, CEM II/A and CEM II/B-Q) after exposure to high temperatures (105 – 500 °C). XRD with subsequent Rietveld analysis was used to quantify the phase composition before and after heating. In addition, the dehydration behavior was analyzed by TGA.

2. Raw materials and sample preparation

Four different cements from the same manufacturer with the same cement clinker classified after DIN EN-197–1 [22], CEM I 42.5 N (96 % clinker, 4 % LS), CEM II/A-LL 42.5 N (86 % clinker, 14 % LS), CEM III/A 42.5 N (56 % clinker, 4 % LS, 40 % BFS) and CEM II/B-Q 42.5 N (72 % clinker, 3 % LS, 25 % CC) were investigated throughout this work. The chemical composition determined by X-ray fluorescence (XRF) analysis and loss of ignition (LOI) provided by the manufacturer compared to the XRF data from measurements carried out independently both according to DIN EN 196–1–2 [23] are shown in Table 1. The XRF measurements at our institution were carried out using a Zetium PANalytical device with a Rh tube anode working in the range of 24–60 kV. For each cement two fused tablets prepared at 1065 °C were used. The $Na_2O_{equiv.}$ corresponds to $Na_2O_{equiv.} = Na_2O + 0.658 \times K_2O$. Table 2 provides an overview of the specific surface area according to Blaine. The cement pastes were prepared with a w/c of 0.47 and cast into prismatic molds (4 ×4 x 16 cm) (Fig. 3a)). After 1 day of curing, the samples were demolded and kept in a water bath for 6 more days and then stored in a climate chamber at (20 ± 2) °C and (65 ± 5) % RH until they reached an age of > 180 days. The conditioning time meets the duration recommended by RILEM TC 256-SPF for fire testing [24], consistent with the procedure applied in our previously conducted spalling experiments [20]. In this study, particular attention was given to ensure that the hydration conditions of the cement paste closely matched those of the concrete fire-test specimens. This approach aimed to achieve a comparable degree of hydration, albeit at the expense of potentially increased carbonation, since previous research has shown that saturated or sealed curing conditions significantly affect both the degree of hydration and the associated moisture distribution [25–27], factors considered critical for explosive concrete spalling.

For the XRD analysis with Rietveld refinement, samples of the four cements and the cement pastes were prepared both before and after high temperature treatment. Before the high-temperature treatment, four sub-samples of almost equal size were obtained by splitting the prisms with a hydraulic stone press (Fig. 3b)). Thereafter, the cubic samples were gradually heated at 2 K/min in a drying cabinet from Memmert under atmospheric conditions to target temperatures of 105 °C and 300 °C. The exposure to 500 °C at 2 K/min was carried out in a Carbolite muffle furnace, Type CWF 11/23/E301, also under atmospheric conditions. Once the respective target

Table 1
Chemical composition determined by XRF of the cements provided by the manufacturer (man.) and the chemical composition determined by XRF independently (lab.).

Oxide [wt.-%]	CEM I		CEM II/A-LL		CEM III/A		CEM II/B-Q	
	man.	lab.	man.	lab.	man.	lab.	man.	lab.
SiO_2	18.73	19.84	16.98	18.38	24.85	26.44	32.35	33.99
Al_2O_3	5.01	5.11	4.44	4.81	7.02	7.29	8.31	8.38
Fe_2O_3	3.22	2.99	2.74	2.67	2.38	1.91	3.14	3.00
CaO	61.65	61.88	59.68	60.67	52.39	52.47	46.29	45.58
MgO	3.10	2.89	3.08	3.19	5.01	4.94	2.42	2.50
SO_3	3.06	3.27	3.11	3.34	3.08	3.93	2.31	2.48
K_2O	1.04	1.01	0.91	0.96	0.84	0.94	1.33	1.26
Na_2O	0.21	0.25	0.17	0.22	0.25	0.30	0.21	0.21
Cl	0.05	-	0.06	-	0.06	-	0.04	-
P_2O_5	0.27	0.21	0.28	0.21	0.21	0.16	0.21	0.22
CO_2	1.90	-	6.30	-	1.69	-	1.44	-
H_2O	0.71	-	0.70	-	0.62	-	0.82	-
LOI	**2.61**	**2.07**	**7.0**	**4.60**	**2.31**	**0.93**	**2.26**	**0.94**
Na_2O equiv.	0.89	0.91	0.77	0.85	0.80	0.92	1.08	1.03

Table 2
Specific surface area according to Blaine.

Cement	CEM I	CEM II/A-LL	CEM III/A	CEM II/B-Q
Blaine value [cm^2/g]	2900	4650	4890	6050

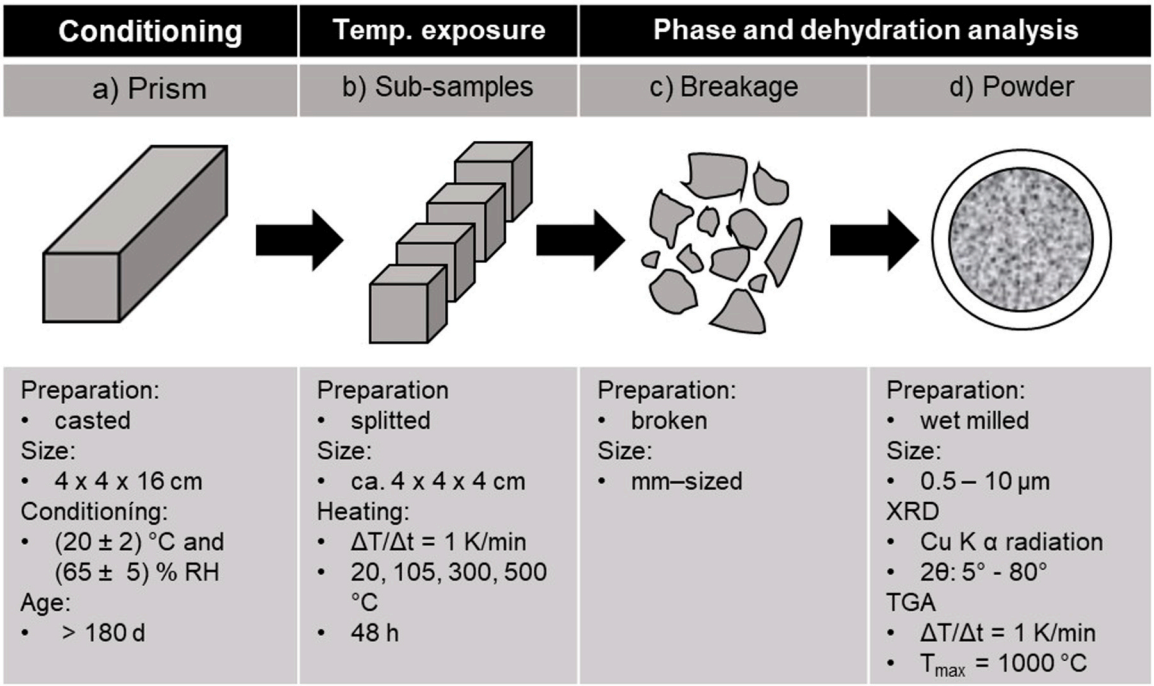

Fig. 3. Sample preparation steps of the hardened cement paste samples.

temperature was reached, it was maintained for 48 h. Even tough tunnel fires can last for such long periods of time (e.g. Mont Blanc Tunnel fire 1999) [28], spalling is usually only expected in the first 20 min. However, the extended heating period was selected to ensure a uniform temperature distribution and complete phase transformation throughout the relatively thick specimen, as hardened cement paste exhibits very low thermal diffusivity which decreases further as temperature rises [29,30]. This approach guarantees that the subsequent XRD analyses are performed on samples that are as homogeneous as possible and free from inhomogeneities caused by incomplete phase transformations due to insufficient temperature equilibration. The temperature gradient that occurs during a real fire and the associated phase composition gradient can thus be analyzed in single steps to understand the cement type specific transformations and their impact on spalling. Further carbonation is not expected, since the rate of carbonation decreases rapidly above 100 °C as with continuous temperature exposure necessary water becomes unavailable [31]. Thereupon, the samples were sealed in plastic wrap and stored in a desiccator to minimize the effects of rehydration. In the next step, the samples were first coarsely crushed (Fig. 3c)) and then finely ground using a McCrone Micronizing Mill (Fig. 3d)). Anhydrous isopropanol was used as the milling medium and was subsequently removed by drying. The milling process lasted 6 min, resulting in a powder with a particle size range between 0.5 – 10 µm [32]. An overview of the sample matrix is given in Table 3. The TGA analysis of the four hardened cement pastes was conducted using residual material from the samples prepared for XRD, prior to any high-temperature exposure.

Table 3
Overview of the sample matrix including the non-hydrated cements and hardened cement pastes exposed to different temperatures.

Material	Sample			
Cement	CEM I	CEM II/A-LL	CEM III/A	CEM II/B-Q
Hardened cement paste	CEM I_20C	CEM II/A-LL_20C	CEM III/A_20C	CEM II/B-Q_20C
	CEM I_105C	CEM II/A-LL_105C	CEM III/A_105C	CEM II/B-Q_105C
	CEM I_300C	CEM II/A-LL_300C	CEM III/A_300C	CEM II/B-Q_300C
	CEM I_500C	CEM II/A-LL_500C	CEM III/A_500C	CEM II/B-Q_500C

3. Methodology

3.1. XRD

The XRD measurements for quantitative analysis of the mineral phases were performed on a Bruker D8 DaVinci diffractometer equipped with an energy dispersive LynxEye detector. The X-ray generator was operated at 40 kV and 25 mA using Cu Kα radiation. Data were collected over a 2θ range of 5° to 80°, with a step size of 0.011° and a counting time of 0.5 s per step. One measurement per sample was performed and deemed sufficient, as repeat measurements of random samples from the same batch showed very good agreement. Rietveld refinement was carried out using **TOPAS V7.0**. The crystal structures used are listed in Table 4 along with their corresponding Inorganic Crystal Structure Database (ICSD) codes. Where no ICSD code is available, the corresponding original literature reference is provided. In anhydrous cement, the typical accuracy is 0.6 – 2 wt% for clinker minerals, 2 wt% for amorphous phases and 0.3 wt% for the residual constituents [33,34]. In the hydrated state, the error for C-S-H content is assumed to be ± 4 wt% [35]

3.2. TGA

Thermogravimetric analysis to investigate the dehydration behavior of the cement paste was also performed twice on ground samples from the same batch used for the XRD samples of each cement type. Roughly 10 mg per sample was measured in a TGA/DSC 3 from Mettler Toledo and heated under a nitrogen (N_2) atmosphere at a heating rate of 10 K/min from 25 °C to 1000 °C.

4. Results

4.1. XRD

The measured XRD patterns of the raw cement are shown in Fig. 4 with the corresponding quantitative phase content displayed in Table 5. The amount of clinker phases decreases with increasing substitution rates of SCMs in the different cement types. Anhydrite and Basanite were identified as sulfate carriers in every cement with slightly different amounts. Moreover, calcite was also found in every sample. For CEM I, CEM III/A and CEM II/B-Q calcite only functioned as a secondary component and therefore appeared in low amounts between 2.5 and 5 wt%. In CEM II/A-LL calcite functioned as the main replacement material for the cement clinker and therefore higher contents of 14 wt% were measured. Additional differences can be seen in the contents of amorphous phases. CEM III/A shows the largest amount of amorphous phase which comes from the replacement of clinker with blast furnace slag. In CEM II/B-Q comparably high fractions of amorphous phases can be seen, caused by the addition of calcined ilitic-kaolinitic clay, which also accounts for the large amounts of quartz present and traces of mica.

The results of the XRD analysis of the hardened cement pastes are presented in Fig. 5. Table 6 provides an overview of the phase composition of all hardened cement pastes analyzed in the initial state (20 °C) and after exposure to 105, 300 and 500 °C. As expected, large residual amounts of the clinker minerals C_3S, C_2S, C_3A and C_4AF were found in the CEM I_20C due to the highest proportion of cement clinker and the coarse grain size distribution associated with the smallest specific surface area according to Blaine. CEM II/A-LL_20C paste showed the second most amount of those phases as it has the second highest amount of clinker and the second smallest Blaine value. In CEM III/A_20C and CEM II/B-Q_20C barely any clinker minerals were left, indicating a near complete hydration. In addition, calcite was detected in all samples as it was a secondary component of the cements. However, increasing amounts of calcium carbonate with the appearance of vaterite was caused by carbonation of the samples. The tendency of increasing calcite contents in comparison to the non-hydrated cement are caused by the transition of metastable vaterite into calcite [36]. Especially hardened

Table 4
Crystal structures and their corresponding ICSD codes.

Phase	ICSD Code
C_3S	94742
C_2S	963
C_3A cubic	1841
C_3A orthorhombic	100220
C_4AF	9197
Anhydrite	16382
Bassanite	79529
Ettringite	155395
Hemicarbonate	263
Monocarbonate	59237
Monosulfate	100138
C-S-H	Bergold et al. [35]
Portlandite	34241
Calcite	80869
Vaterite	15879
Quartz	174

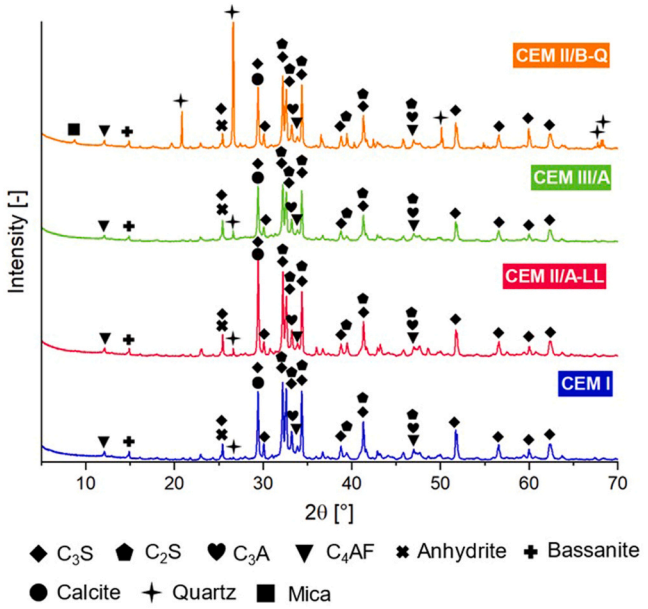

Fig. 4. XRD patterns of the different cements.

Table 5
Phase composition of the cements used [wt%].

Mineral phase	CEM I	CEM II/A-LL	CEM III/A	CEM II/B-Q
C_3S	50.0	47.0	32.0	40.0
C_2S	13.0	10.0	7.0	4.0
C_3A	9.8	7.5	5.4	6.7
C_4AF	6.2	5.8	3.9	1.2
Anhydrite	2.0	1.8	1.2	1.1
Bassanite	1.2	1.4	1.1	1.5
Calcite	5.0	14.0	3.8	2.5
Quartz	0.3	0.7	0.8	16.0
Amorphous	7.8	6.2	42.0	14.5
Others	4.5	4.8	2.7	8.2

cement pastes of CEM III/A and CEM II/B-Q showed high contents of carbonate phases suggesting a stronger degree of carbonation, which is often observed in slag or calcined clay cement blends [37,38]. After exposure to 500 °C, parts of the vaterite tend to decompose, while calcite remains stable which is consistent with previous findings of Li et al. [39]. This phenomenon occurs due to the lower lattice packing density of vaterite in comparison to calcite [40]. Another noticeable point is the significant amounts of quartz (at least 12 wt%) found in the CEM II/B-Q cement paste samples which is a byproduct from the calcined clay.

Lower amounts of AFt and AFm phases (hemicarboaluminate, monocarboaluminate and monosulfoaluminate) were identified in the blended cement pastes (CEM II/A-LL_20C, CEM III/A_20C and CEM II/B-Q_20C) ranging between 8.5 and 9.0 wt%, compared to 11.6 wt% in CEM I_20C. After an exposure to 105 °C, ettringite dehydrated and is no longer visible in the XRD patterns. A further temperature increase to 300 °C led to the dehydration and decomposition of all AFm phases in every sample.

Lower amounts of C-(A)-S-H were identified in CEM III/A and CEM II/B-Q hardened pastes, with values of 22 and 23 wt%, respectively, compared to approximately 30 wt% in CEM I and CEM II/A-LL hardened pastes. However, the thermal stability of the C-(A)-S-H phases varied among the different cement types. While the C-(A)-S-H in CEM I_300C and CEM II/A-LL_300C underwent significant dehydration between 105 °C and 300 °C and was almost completely decomposed after exposure to 500 °C, the C-(A)-S-H in CEM II/B-Q_300C and particularly in CEM III/A_300C remained stable up to 300 °C. Near-complete dehydration and decomposition were only observed after exposure to 500 °C in CEM III/A_500C and CEM II/B-Q_500C. The increased thermal stability of slag cement paste was also reported by Jia et al. [41] and might be associated with the formation of more tightly packed C-(A)-S-H gels. Beside the C-S-H content the amount of portlandite also varied between the single cement pastes. Lower portlandite contents of around 5 wt% were observed throughout the CEM III/A and CEM II/B-Q hardened cement paste samples, while higher amounts of approximately 10 and 8 wt% were recorded in CEM I and CEM II/A-LL samples respectively. These differences are caused by the lower amounts of available clinker minerals and the pozzolanic reaction of the slag and calcined clay containing binders. Even after exposure to 500 °C, portlandite always appeared in the XRD patterns. However, the detected peaks decreased in height, but increased in width with rising temperature exposure, which indicates a decline in crystallinity but no complete degradation of the structure. Hence, despite the

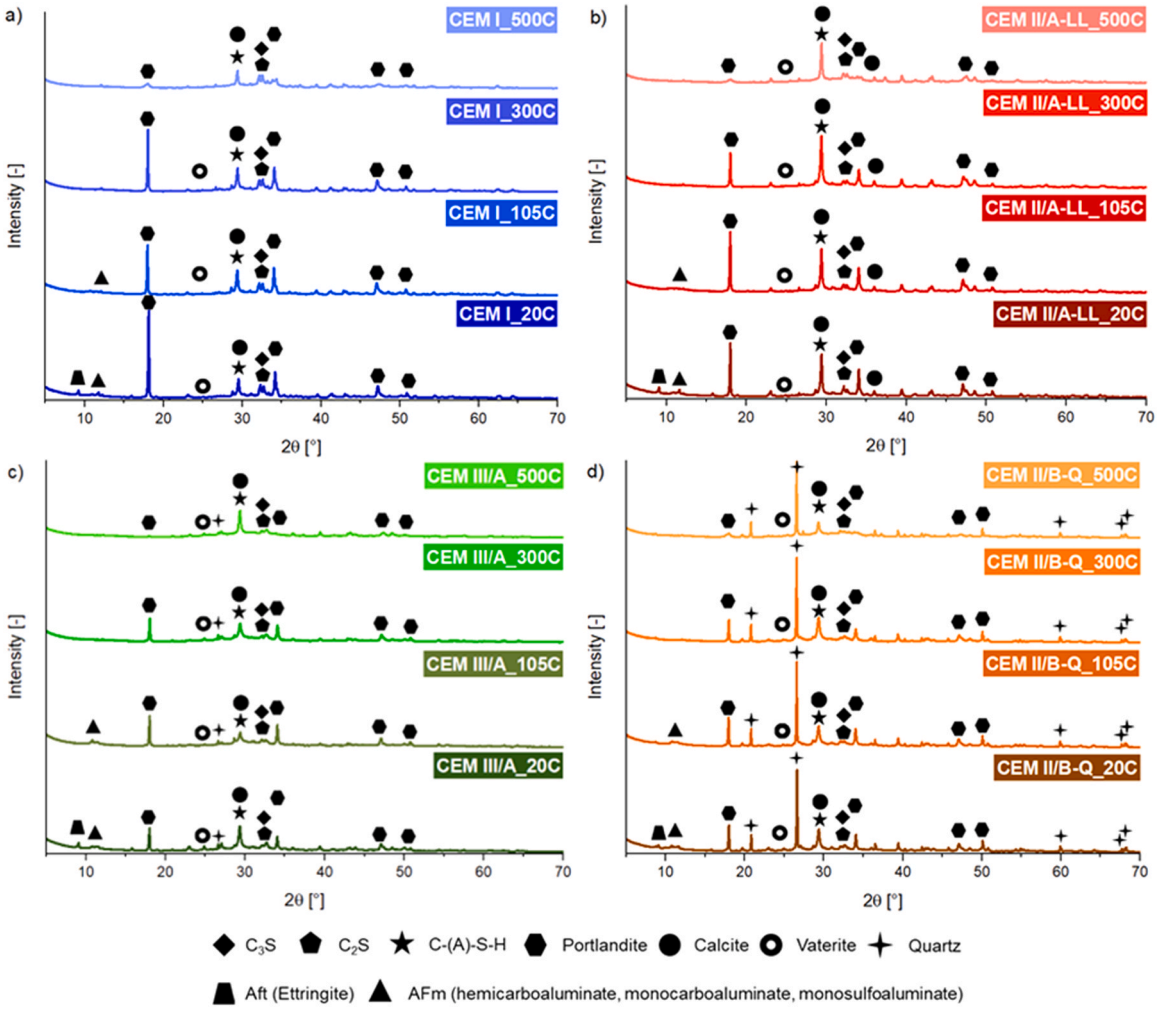

Fig. 5. XRD patterns of the different hardened cement pastes after exposure to 20 °C, 105 °C, 300 °C and 500 °C.

occurring dehydration the crystal structure remains detectable, similar findings were reported by Song et al. [6]. Interestingly, CEM III/A_500 C exhibited a more pronounced decomposition of portlandite. The underlying cause remains uncertain; however, previous studies have shown that the phase assemblage of the non-hydrated cement and chemical environment during hydration can influence its size and morphology [42,43], which may also affect the thermal stability of portlandite. Overall, crystallinity decreased after temperature exposure to 500 °C, caused mainly by the dehydroxylation of C-(A)-S-H leading to an increase of the amorphous phase content. The high content of amorphous phases in hardened CEM III/A paste is based on the residual content of blast furnace slag, which generally reacts to only about 40 % after a hydration period of 6 months [44].

4.2. TGA

Fig. 6 shows the results of the TGA for the different hardened cement pastes. Because of the solvent exchange during the sample preparation with isopropanol no free evaporable water remained. The water loss up to 200 °C can be mainly attributed to the dehydration of AFt and AFm phases. Here, the largest mass loss was recorded in the CEM I_20C sample, which corresponds to the XRD measurements where the most amounts of AFt and AFm phases were found. For CEM II/B-Q_20C a noticeable increase in water loss was displayed between 140 and 200 °C, which can be attributed to AFm phases (most likely monocarboaluminate). Furthermore, CEM III/A_20C cement paste shows the lowest mass loss over the temperature increase up to 500 °C, which would support the idea of a thermally more stable C-(A)-S-H phase in the slag cement also seen in the XRD results. Between 400 °C and 500 °C the dehydration of portlandite was observed, resulting in a comparatively lower mass loss in the latent hydraulic and pozzolanic cementitious systems. The relatively low temperature onset of dehydration suggests low crystallinity of the portlandite phase. Lastly, the decomposition of calcium carbonate was detected already between 500 and 760 °C. A closer look into the differential thermal gravimetry (DTG) showed a two stage mass loss associated with the decomposition of calcium carbonate, whereas the first is coming from low crystalline vaterite

Table 6
Phase composition in wt% of the hardened cement pastes before and after exposure to temperatures of 105, 300 and 500 °C determined by XRD.

Sample		C_3S	C_2S	C_3A	C_4AF	Ettringite	Hemicarb.	Monocarb.	Monsulf.	C-(A)-S-H	Portlandite	Calcite	Vaterite	Quartz	Amorphous	Others
CEM I	20 C	5.8	7.0	2.0	3.6	4.0	1.6	5.7	0.3	30.0	9.0	4.7	4.4	0.3	20.8	0.8
	105 C	6.0	8.0	2.0	3.6	0.0	1.5	3.2	0.4	35.0	10.0	8.8	5.8	0.3	14.4	1.0
	300 C	6.8	8.0	2.0	4.0	0.0	0.0	0.3	0.0	21.0	11.0	8.8	4.9	0.5	31.7	1.0
	500 C	7.0	9.0	2.0	3.3	0.0	0.0	0.0	0.0	10.0	9.0	7.0	0.5	0.4	50.8	1.0
CEM II/A-LL	20 C	2.0	3.8	1.0	2.3	2.7	1.0	4.8	0.0	30.0	8.5	12.6	4.6	0.4	25.1	1.2
	105 C	2.0	4.0	1.0	2.9	0.0	0.9	3.0	0.4	34.0	9.4	14.0	3.5	0.5	23.2	1.2
	300 C	2.0	4.0	1.1	1.7	0.0	0.0	0.0	0.0	21.0	7.6	25.0	6.0	0.4	29.7	1.5
	500 C	2.0	5.0	1.0	1.5	0.0	0.0	0.0	0.0	5.0	7.0	18.0	1.0	0.4	57.7	1.4
CEM III/A	20 C	0.7	1.2	0.2	1.0	3.5	1.0	4.0	0.0	22.0	4.0	7.1	11.0	0.7	43.0	0.6
	105 C	0.8	2.0	0.2	1.2	0.0	1.6	3.2	0.0	21.0	5.0	2.5	3.0	0.5	58.5	0.5
	300 C	0.5	2.0	0.2	1.3	0.0	0.0	0.0	0.0	22.0	6.0	5.0	8.0	0.7	53.6	0.7
	500 C	0.8	2.4	0.2	1.4	0.0	0.0	0.0	0.0	7.0	0.1	14.0	9.0	0.5	63.9	0.7
CEM II/B-Q	20 C	0.4	2.0	0.5	1.2	1.3	1.5	5.2	1.0	23.0	4.5	8.0	10.0	12.0	24.8	4.0
	105 C	0.8	2.0	0.0	1.7	0.0	1.2	5.2	0.0	28.0	5.7	8.0	7.5	13.0	21.8	5.1
	300 C	0.9	2.0	0.0	1.5	0.0	0.0	0.0	0.0	21.0	4.7	12.0	10.0	14.0	29.0	4.9
	500 C	1.0	2.0	0.2	0.4	0.0	0.0	0.0	0.0	7.0	4.8	6.0	2.5	14.0	56.4	5.7

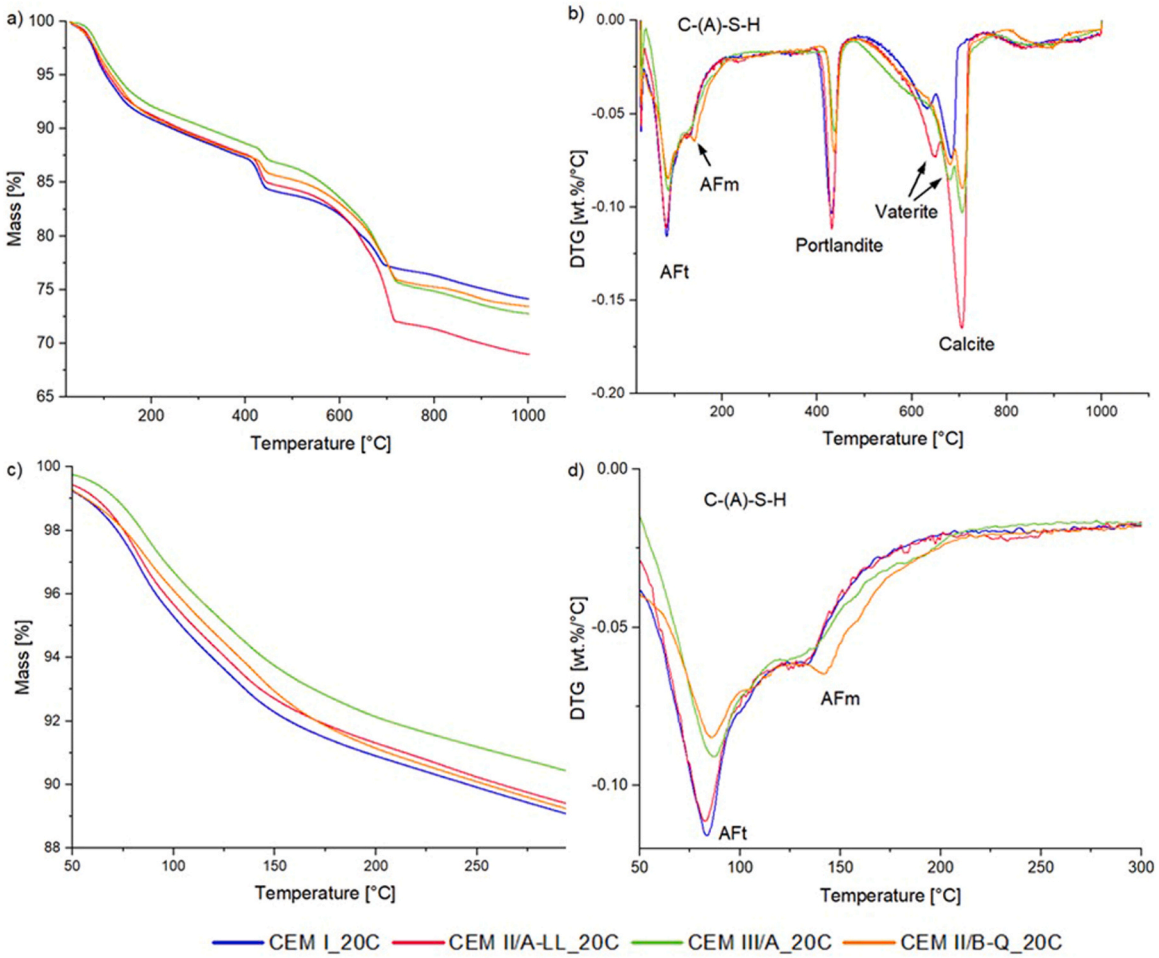

Fig. 6. Thermal analysis of the hardened cement pastes a) TGA 20–1000 °C; b) DTG 20–1000 °C; c) TGA 50–300 °C; d) DTG 50–300 °C.

and amorphous calcium carbonate present due to carbonation [39]. This also explains why the decomposition started at comparably low temperatures, where it would be not expected for pure and well crystalline calcite [39]. The overall mass loss associated with calcium carbonate was obviously the most pronounced for CEM II/A-LL_20C. However, both CEM III/A_20C and CEM II/B-Q_20C exhibit a higher mass loss than the CEM I paste, despite having similar initial calcium carbonate contents. This was attributed to more pronounced carbonation in the blended cement paste samples. This observation is consistent with the XRD results, which showed the highest amounts of vaterite in the CEM III/A_20C and CEM II/B-Q_20C samples. Up to 500 °C, the CEM I paste showed the relative highest mass loss (which was solely attributed to dehydration) of 16.2 wt% followed by CEM II/A-LL_20C, CEM II/B-Q_20C and CEM III/A_20C with 15.64, 14.76, and 13.60 wt% respectively. The final relative mass loss after thermal exposure to 1000 °C was highest in the CEM II/A-LL_20C at 31.08 wt% followed by CEM II/B-Q_20C (26.60 wt%), CEM III/A_20C (27.28 wt%) and CEM I_20C (25.91 wt %). This trend is attributed to the decomposition of carbonate phases.

5. Discussion

The analysis of the phase composition and dehydration behavior of the cement pastes was carried out to gain deeper insight into the increased spalling susceptibility observed for blended cement concretes. This study revealed clear differences in both phase content and decomposition behavior. The behavior of the hydrate phases up to around 300 °C plays a particular role, as this temperature range is typically associated with explosive spalling. It was observed that CEM I cement pastes tend to have higher amounts of combined AFt and AFm phases, which already dehydrate between 70 and 200 °C. This might have a positive impact, lowering the spalling susceptibility in OPC concrete since more water can be released at comparable moderate temperatures before spalling occurs. All cement pastes exhibit carbonation, with more pronounced carbonation observed in CEM III/A and CEM II/B-Q samples. This is occurs more rapidly in C-(A)-S-H due to reduced portlandite contents [41]. Furthermore, CEM I and CEM II/A-LL showed higher contents of C-(A)-S-H in comparison to CEM III/A and CEM II/B-Q. The XRD results recorded after high temperature exposure showed that C-(A)-S-H in CEM II/B-Q and particularly in CEM III/A paste is thermally more stable, which was also confirmed by the TGA

measurements retaining more water and structural stability at higher temperatures. This is also in alignment with observations reported by Xu et al. [45] who concluded that the 'dreierketten'-like structure of C-(A)-S-H in slag blended cement systems remains stable up to 450 °C. Responsible for this increased thermal stability might be the more tightly packed structure of C-(A)-S-H gels [41] which incorporate higher amounts of non-evaporable water [46]. In addition, the increased carbonation of the C-(A)-S-H phases due to less portlandite contents [47] can lead to the formation of calcium-carbonate modified silica gel, which shows increased high-temperature resistance [39]. However, this effect would only affect the first few centimeters in large concrete structures and therefore is less relevant for explosive spalling. The improved thermal stability of C-(A)-S-H in slag- or pozzolan-containing systems may contribute to enhanced mechanical performance at elevated temperatures, as reported in literature [48,49]. However, our observations indicate a more pronounced increase in permeability after exposure to 150 °C in concrete samples produced with the same cements (Table 7) [21]. This suggests that the increase is not due to more severe degradation of the cementitious matrix. Instead, other factors, such as pore pressure and the associated development of microcracks, may be responsible for this phenomenon. Currently, no experimental data on pore pressure in concretes with these cements are available; however, numerical simulations by Peters et al. [50] based on the same cements indicate a slight increase in pore pressure for CEM III/A and CEM II/B-Q concrete in comparison to CEM I concrete. Additionally, simulations by Jia et al. [51] concluded that the incorporation of fly ash influences pore pressure and crack development in cementitious materials. Furthermore, Reiners et al. [19] reported that concrete made with blended cements exhibits a less distinct interfacial transition zone (ITZ). As a result, there is no effective "cushion" to accommodate the expansion of aggregates, leading to more severe cracking in slag and pozzolan containing concretes. Both aspects may explain the observed competing effects: increased thermal stability of the cementitious matrix coupled with a steeper rise in permeability at elevated temperatures.

In our previous study, we showed that the development of the drying front and permeability in concrete changes with the cement type used [21]. The detected moisture profiles after heating correlate very well with the dehydration behavior of the hardened cement pastes, meaning that the sequence of drying from the least progressed in CEM III/A to the most progressed in CEM I matches with the sequence of mass loss determined by TGA up to 216 °C (Fig. 7). At higher temperatures, it appears as if the drying behavior shown in the ^{1}H NMR relaxometry measurements is the same in all types of concrete. This is because the NMR tomograph cannot fully detect chemically bound water, thus, further differences only appear in the mass loss obtained by TGA. The comparison indicates that the thermally induced moisture transport is consistent with dehydration behavior of the cementitious matrix. Furthermore, this explains why CEM III/A and CEM II/B-Q concrete exhibit very different drying behaviors despite having the same initial moisture content and permeability development as described in [21] (see Table 7). In this regard, it should also be added that the increase in permeability at higher temperatures has probably only minor impact on the drying behavior, as most of the water is already released up to 200 °C. It must be noted that the correlation between cement mass loss and the progression of the drying front can only be considered indirect. In concrete, additional factors, such as the quantity and type of aggregates, the ITZ, and the resulting crack formation also play a significant role. Furthermore, in a real concrete component, constraints and applied loads must be taken into account, as they can influence the structural behavior and thermomechanical response.

In summary, the results lead to the hypothesis that stronger water retention during heating in blended cement concrete, caused by thermally more stable hydrate phases, increases the risk of spalling, as more moisture remains available before the onset of the moisture clog. Although the observed moisture differences appear minor, previous research has demonstrated that even slight increases in moisture content can significantly raise spalling susceptibility, even when permeability is constant [52].

6. Conclusion

The analysis of the thermally induced phase decomposition in blended cement pastes showed clear differences between the individual cement pastes. Regarding explosive spalling of concrete, the following conclusions were drawn:

- All blended cement pastes tend to show lower amounts of early dehydrating AFt and AFm phases in comparison to CEM I paste observed in the XRD results. The TGA showed similar tendencies, with a slightly higher water loss for CEM I paste. In blended cement concrete lower permeabilities further inhibit water release leading to more available moisture in a temperature range critical for explosive spalling.
- The C-(A)-S-H in blended cements with latent hydraulic or pozzolanic properties showed better thermal stability especially in CEM III/A paste, since less decomposition was recorded over increasing temperatures. The increased thermal stability might be caused by the denser structure of C-(A)-S-H gels as well as their enhanced carbonation which may lead to the formation of calcium-modified silica gels with improved thermal properties.
- The drying behavior and associated moisture transport in blended cement concrete is strongly determined by the dehydration behavior of the cementitious matrix up to 200 °C. The development, particularly the different increase of permeability with increasing temperatures seems to play a less significant role as most of the water is already released below 200 °C. Therefore, the initial permeability is more decisive for evaluating the spalling risk of concrete.
- The increased thermal stability of hardened cement pastes containing slag and calcined clays is often considered beneficial for concrete strength at high temperatures, however, the opposite is true for fire-induced spalling. Therefore, its use in practice must be carefully considered if fire resistance is required.

7. Outlook

Besides the impact on the thermohydraulic mechanism, the cement type might also influence the thermomechanical behavior of

Table 7
Intrinsic gas permeability of the different concretes after exposure to 20 °C, 105 °C, 150 °C, 170 °C and 300 °C [21].

Intrinsic permeability		CEM I	CEM II/A-LL	CEM III/A	CEM II/B-Q
Permeability $K_{gas(20\ °C)}$		2.13×10^{-17}	5.86×10^{-18}	2.19×10^{-18}	5.47×10^{-18}
Permeability $K_{gas(105\ °C)}$		1.55×10^{-16}	3.49×10^{-17}	3.10×10^{-17}	3.31×10^{-17}
Permeability $K_{gas(150\ °C)}$	[m^2]	2.36×10^{-16}	7.69×10^{-17}	1.04×10^{-16}	1.43×10^{-16}
Permeability $K_{gas(170\ °C)}$		3.20×10^{-16}	1.20×10^{-16}	1.65×10^{-16}	2.05×10^{-16}
Permeability $K_{gas(300\ °C)}$		1.16×10^{-15}	4.88×10^{-16}	1.17×10^{-15}	9.99×10^{-16}

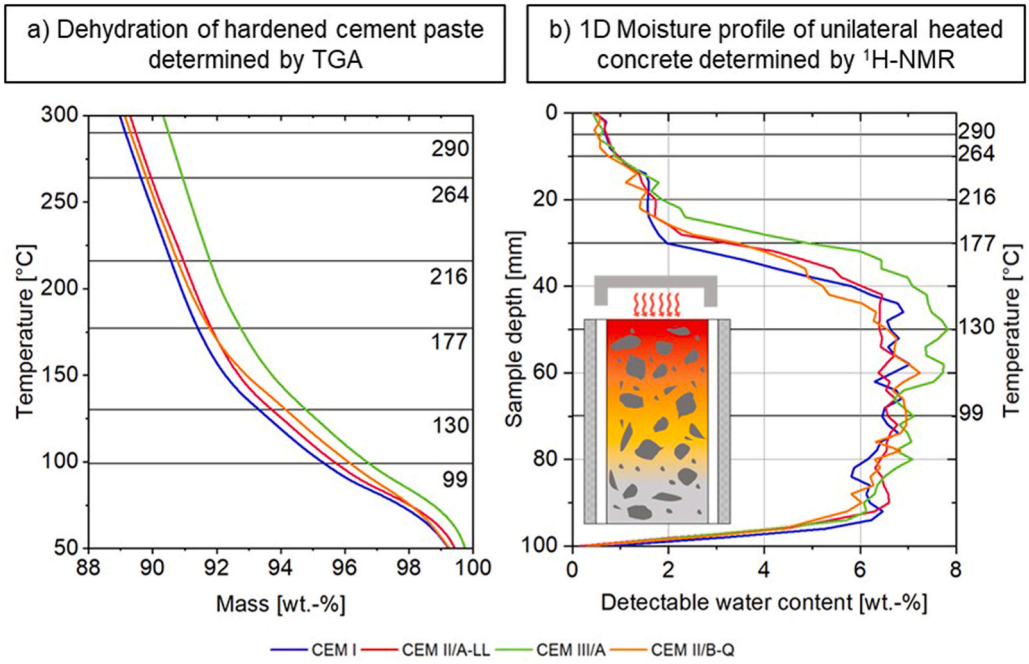

Fig. 7. Comparison between a) the dehydration behavior of the hardened cement pastes (TGA) and b) the moisture profiles in concrete made with the corresponding cement after one sided heating (^{1}H NMR) described in [21] shows the same sequence of water loss.

concrete.

The increased thermal stability of C-(A)-S-H in CEM II/B-Q and CEM III/A might lead to different thermomechanical behaviors particularly with regard to load-induced thermal strains (LITS). In concrete structures where thermal deformations are usually partially or completely restrained, LITS have a positive influence. LITS act in the direction of the applied load and therefore reduce compressive stresses caused by the restrained thermal expansion [53] potentially lowering the risk of explosive spalling. Key mechanisms behind the formation of LITS are thermal transient creep and drying creep, which are both strongly dependent on the decomposition of the hydrate phases and the associated water transport [54,55]. Peters et al. [56] observed that the evolution of the degree of C-S-H dehydration is in close agreement with experimentally determined evolution of LITS caused by creep-like C-S-H sliding under compressive load. Thermally stable C-(A)-S-H found in CEM II/B-Q and CEM III/A paste might inhibit this effect, leading to lower LITS and lower relaxation rates of thermally induced stresses. Hence, increasing the spalling susceptibility in blended cement concrete made with those types of cement.

Furthermore, the thermal mismatch between the shrinking cement matrix and the expanding aggregates at elevated temperatures (around 150 °C) is considered to be a key factor for explosive concrete spalling. The mismatch generates internal stresses that tend to promote spalling. The shrinkage behavior of pure cement paste progresses through four distinct stages according to Koyama et al. [57]: Initially, between 20 °C and 140 °C, shrinkage begins due to the evaporation of free water and the dehydration of AFt phases. This is followed by a steady shrinkage phase from 140 °C to 300 °C, driven by the loss of interlayer water from the C-S-H gel. Between 300 °C and 490 °C, shrinkage accelerates significantly due to further water loss. Finally, in the stabilization stage beyond 490 °C, C-S-H begins to recrystallize, which reduces further contraction. In blended cement pastes, however, the composition of residual non-hydrated phases varies considerably and should not be neglected. For example, the CEM II/B-Q cement examined in this study contains a high proportion of quartz, which can be considered micro-aggregates. This introduces thermal incompatibility even at the binder level. Quartz aggregates exhibit a particularly pronounced thermal mismatch, but similar effects are also observed with limestone and slag aggregates [58]. The impact of these factors should not be overlooked when assessing the influence of cement type on explosive spalling, especially when aiming for a comprehensive and holistic understanding.

In the future, investigations based on the present results should take a closer look at the thermo-mechanical behavior of blended cement concrete in order to verify or reject the hypotheses regarding the differences in LITS and the thermal mismatch between the cement constituents mentioned above.

CRediT authorship contribution statement

Frank Dehn: Writing – review & editing, Supervision. **Frank Weise:** Writing – review & editing, Supervision, Resources, Project administration, Funding acquisition, Conceptualization. **Ludwig Stelzner:** Writing – review & editing, Supervision, Resources, Project administration, Funding acquisition, Conceptualization. **Tim Pittrich:** Writing – review & editing, Writing – original draft, Visualization, Investigation, Formal analysis, Conceptualization. **Daniel Jansen:** Writing – review & editing, Resources, Investigation, Formal analysis.

Declaration of Competing Interest

The authors declare the following financial interests/personal relationships which may be considered as potential competing interests: Tim Pittrich reports financial support was provided by German Research Foundation. If there are other authors, they declare that they have no known competing financial interests or personal relationships that could have appeared to influence the work reported in this paper.

Acknowledgements

We gratefully acknowledge the support of the German Research Foundation (DFG) and extend our gratitude for their financial support throughout the project ‘‘Thermohydraulic spalling mechanisms in concretes with different binders with and without PP fibers under fire exposure: An experimental and numerical analysis’’ (Project Nr. 491928256). We also express our sincere appreciation to our colleagues, specifically acknowledging the collaborative efforts of BAM divisions 6.3: Structure Analysis, 7.1: Building Materials, and 7.4: Technology of Construction Materials. Their expertise and resources have significantly enriched the scope and depth of our study.

Data availability

Data will be made available on request.

References

[1] K.L. Scrivener, J.M. Vanderley, E.M. Gartner, Eco-efficient cements: Potential economically viable solutions for a low-CO2 cement-based materials industry, Cem. Concr. Res 114 (2018) 2–26, https://doi.org/10.1016/j.cemconres.2018.03.015.
[2] B. Lothenbach, K. Scrivener, R.D. Hooton, Supplementary cementitious materials, Cem. Concr. Res 41 (2011) 1244–1256, https://doi.org/10.1016/j.cemconres.2010.12.001.
[3] McNamee R. (2019) Fire Spalling Theories - Realistic and More Exotic Ones. Proceedings of the 6th International Workshop on Concrete Spalling due to Fire Exposure: Sheffield, England.
[4] T. Pittrich, F. Weise, L. Stelzner, The impact of blended cements on the spalling behavior of concrete at elevated temperatures: a review, Mater. Struct. 58 (2025), https://doi.org/10.1617/s11527-025-02713-x.
[5] I. Hager, Behaviour of cement concrete at high temperature (Technical Sciences), Bull. Pol. Acad. Sci. 61 (2013), https://doi.org/10.2478/bpasts-2013-0013.
[6] H. Song, Y. Jeong, S. Bae, et al., A study of thermal decomposition of phases in cementitious systems using HT-XRD and TG, Constr. Build. Mater. 169 (2018), https://doi.org/10.1016/j.conbuildmat.2018.03.001.
[7] Q. Zhang, G. Ye, Quantitative analysis of phase transition of heated Portland cement paste, J. Therm. Anal. Calor. 112 (2013) 629–636.
[8] Saillio M., Sabeur H., Vincent J. et al (2021) Phase assemblage of a 5 year-old cement paste after submission to various high temperature and cooling regime. https://doi.org/10.1016/j.conbuildmat.2021.122440.
[9] M. Saillio, V. Baroghel-Bouny, M. Bertin, et al., Phase assemblage of cement pastes with SCM at different ages, Constr. Build. Mater. 244 (2019) 144–157, https://doi.org/10.1016/j.conbuildmat.2019.07.059.
[10] R.-S. Lin, Y. Han, X.-Y. Wang, Macro–meso–micro experimental studies of calcined clay limestone cement (LC3) paste subjected to elevated temperature, Cem. Concr. Compos 116 (2021), https://doi.org/10.1016/j.cemconcomp.2020.103871.
[11] Y. Cao, Y. Wang, Z. Zhang, et al., Thermal stability of limestone calcined clay cement (LC3) at moderate temperatures 100–400 °C, Cem. Concr. Compos. (2023), https://doi.org/10.1016/j.cemconcomp.2022.104832.
[12] S. Donatello, C. Kuenzel, A. Palomo, et al., High temperature resistance of a very high volume fly ash cement paste, Cem. Concr. Compos 45 (2014), https://doi.org/10.1016/j.cemconcomp.2013.09.010.
[13] L. Xu, J. Wang, K. Li, et al., A systematic review of factors affecting properties of thermal-activated recycled cement, Resour. Conserv. Recycl. 185 (2022), https://doi.org/10.1016/j.resconrec.2022.106432.
[14] N.C. Collier, Transition and Decomposition Temperatures of Cement Phases - A Collection of Thermal Analysis Data, Ceram. -Silik. áty 60 (2016) 338–343, https://doi.org/10.13168/cs.2016.0050.
[15] M. Sundin, H. Hedlund, A. Cwirzen, Eco-Concrete in High Temperatures, Mater 16 (2023), https://doi.org/10.3390/ma16124212.
[16] Kirnbauer J. and Schneider U. (2011) Influence of cement type and aggregate shape on explosive concrete spalling. 2nd International RILEM Workshop on Concrete Spalling due to Fire Exposure: Delft, The Netherlands 432-439.
[17] I. Hager, K. Mróz, T. Tracz, Concrete propensity to fire spalling: Testing and observations, MATEC Web Conf. 163 (2018), https://doi.org/10.1051/matecconf/201816302004.
[18] M.J. Miah, F. Lo Monte, R. Felicetti, et al., Impact of external biaxial compressive loading on the fire spalling behavior of normal-strength concrete, Constr. Build. Mater. 366 (2023), https://doi.org/10.1016/j.conbuildmat.2022.130264.
[19] J. Reiners, J. Zehfuß, F. Dehn, et al., The influence of the physical and chemical properties of hardened cement paste on the heat-induced explosive spalling of concrete, Civ. Eng. Des. 6 (2024) 4–21, https://doi.org/10.1002/cend.202300020.

[20] Pittrich T., Stelzner L. and Weise F. (2024) Fire-induced spalling of normal strength concrete with different types of blended Portland cement. The 13th International Conference on Structures in Fire: Coimbra, Portugal 451-461.
[21] Pittrich T., Peters S., Meschke G. et al (2025) Thermally induced moisture transport in concrete with different types of blended Portland cement studied by ^{1}H NMR relaxometry. https://doi.org/10.21203/rs.3.rs-7913874/v1.
[22] DIN EN 197-1, Cement - Part 1: Composition specifications and conformity for common cements, Beuth Verlag GmbH, Berlin, Germany, 2011.
[23] DIN EN 196-2, Methods of testing cement – Part 2: Chemical analysis of cement, Beuth Verlag GmbH, Berlin, Germany, 2013.
[24] P. Pimienta, R. McNamee, I. Hager, et al., Recommendation of RILEM TC 256-SPF on the method of testing concrete spalling due to fire: material screening test, Mater. Struct. 56 (2023), https://doi.org/10.1617/s11527-023-02202-z.
[25] Bentz D.P., Snyder K.A. and Stutzman P.E. (1997) Hydration of Portland Cement: The Effects of Curing Conditions. Proceedings of the 10th International Congress on the Chemistry: Sweden.
[26] D.P. Bentz, P.E. Stutzman, Curing, Hydration, and Microstructure of Cement Paste, Acids Mater. J. (2006) 348–356.
[27] M. Nematollahzade, A. Tajadini, A. Iman, et al., Influence of different curing conditions and water to cement ratio on properties of self-compacting concretes, Constr. Build. Mater. 237 (2020), https://doi.org/10.1016/j.conbuildmat.2019.117570.
[28] Catmur J., King K., Parsons M. et al (2023) A Service Analysis of the Mont Blanc Tunnel Fire. Safety Critical Systems Symposium:113-145.
[29] K.Y. Shin, S.B. Kim, J.H. Kim, et al., Thermo-physical properties and transient heat transferof concrete at elevated temperatures, Nucl. Eng. Des. 212 (2002) 233–241.
[30] Q. Zhang, D. Yan, Temperature dependence ofthermal diffusivity of OPCand CAC cement paste, Adv. Cem. Res. 28 (2016) 576–582, https://doi.org/10.1680/jadcr.15.00146.
[31] D. Wang, T. Noguchi, T. Nozaki, et al., Investigation of the carbonation performance of cement-based materials under high temperatures, Constr. Build. Mater. 272 (2021), https://doi.org/10.1016/j.conbuildmat.2020.121634.
[32] A.J. Locock, D. Chesterman, D. Caird, et al., Miniaturization of mechanical milling for powder X-ray diffraction, Powder Diffr. 27 (2012) 189–193, https://doi.org/10.1017/S0885715612000516.
[33] G. Walenta, T. Füllmann, M. Gimenez, Quantitative Rietveld analysis of cement and clinker, Int. Cem. Rev. (2001) 51–54.
[34] T. Westphal, G. Walenta, T. Füllmann, et al., Characterisation of cementitious materials— Part III, Int. Cem. Rev. (2002) 47–51.
[35] S.T. Bergold, F. Goetz-Neunhoffer, J. Neubauer, Quantitative analysis of C-S-H in hydrating alite pastes by in-situ XRD, Cem. Concr. Res 53 (2013) 119–126, https://doi.org/10.1016/j.cemconres.2013.06.001.
[36] T. Ogino, T. Suzuki, K. Sawada, The rate and mechanism of polymorphic transformation of clacium carbonate in water, J. Cryst. Growth 100 (1990) 159–167, https://doi.org/10.1016/0022-0248(90)90618-U.
[37] F. Lollini, E. Redaelli, Carbonation of blended cement concretes after 12 years of natural exposure, Constr. Build. Mater. 276 (2021), https://doi.org/10.1016/j.conbuildmat.2020.122122.
[38] R. Bucher, P. Diedrich, G. Escadeillas, et al., Service life of metakaolin-based concrete exposed to carbonation Comparison with blended cement containing fly ash, blast furnace slag and limestone filler, Cem. Concr. Res 99 (2017) 18–29, https://doi.org/10.1016/j.cemconres.2017.04.013.
[39] Y. Li, T. Mi, W. Liu, et al., Chemical and mineralogical characteristics of carbonated and uncarbonated cement pastes subjected to high temperatures, Compos. Part B 216 (2021), https://doi.org/10.1016/j.compositesb.2021.108861.
[40] G. Sun, X. Liu, B. Lian, et al., Research Progress on Vaterite Mineral and Its Synthetic Analogs, Mater 15 (2025), https://doi.org/10.3390/min15080796.
[41] Z. Jia, C. Chen, J. Shi, et al., The microstructural change of C-S-H at elevated temperature in Portland cement/GGBFS blended system, Cem. Concr. Res (2019), https://doi.org/10.1016/j.cemconres.2019.05.018.
[42] E. Gallucci, K. Scrivener, Crystallisation of calcium hydroxide in early age model and ordinary cementitious systems, Cem. Concr. Res 37 (2007) 492–501, https://doi.org/10.1016/j.cemconres.2007.01.001.
[43] S. Galmarini, A. Aimable, N. Ruffray, et al., Changes in portlandite morphology with solvent composition: Atomistic simulations and experiment, Cem. Concr. Res 41 (2011) 1330–1338, https://doi.org/10.1016/j.cemconres.2011.04.009.
[44] V.K. Singh, 17 - Developments in Portland slag cements. Woodhead Publishing Series in Civil and Structural Engineering, The Science and Technology of Cement and Other Hydraulic Binders, Woodhead Publishing, 2023, pp. 625–651.
[45] L. Xu, J. Wang, K. Li, et al., New insights on dehydration at elevated temperature and rehydration of GGBS blended cement, Cem. Concr. Compos. 139 (2023), https://doi.org/10.1016/j.cemconcomp.2023.105068.
[46] E. Kapeluszna, Ł. Kotwica, A. Rózycka, et al., Incorporation of Al in C-A-S-H gels with various Ca/Si and Al/Si ratio: Microstructural and structural characteristics with DTA/TG, XRD, FTIR and TEM analysis, Constr. Build. Mater. 155 (2017) 643–653, https://doi.org/10.1016/j.conbuildmat.2017.08.091.
[47] S. von Greve-Dierfeld, B. Lothenbach, A. Vollpracht, et al., Understanding the carbonation of concrete with supplementary cementitious materials: a critical review by RILEM TC 281-CCC, Mater. Struct. 53 (2020), https://doi.org/10.1617/s11527-020-01558-w.
[48] H. Seleem, A.M. Rashad, T. Elsokary, Effect of elevated temperature on physico-mechanical properties of blended cement concrete, Constr. Build. Mater. 25 (2011) 1009–1017, https://doi.org/10.1016/j.conbuildmat.2010.06.078.
[49] A. Savva, P. Manita, K.K. Sideris, Influence of elevated temperatures on the mechanical properties of blended cement concretes prepared with limestone and siliceous aggregates, Cem. Concr. Compos 27 (2005) 239–248, https://doi.org/10.1016/j.cemconcomp.2004.02.013.
[50] S. Peters, T. Pittrich, L. Stelzner, et al., Model based evaluation of effects of the composition of CO2 -reduced blended concrete on the chemo-thermo-hygral behavior at elevated temperatures, Cem. Concr. Compos. 163 (2025), https://doi.org/10.1016/j.cemconcomp.2025.106163.
[51] W. Jiang, D. Zhang, X. Zheng, et al., Development of Pore Pressure in Cementitious Materials under Low Thermal Effects: Evidence from Optimization of Pore Structure by Incorporation of Fly Ash, Mater 16 (2023), https://doi.org/10.3390/ma16124214.
[52] M. Maier, M. Zeiml, R. Lackner, On the effect of pore-space properties and water saturation on explosive spalling of fire-loaded concrete, Constr. Build. Mater. (2020), https://doi.org/10.1016/j.conbuildmat.2019.117150.
[53] G. Torelli, P. Mandal, M. Gillie, et al., Concrete strains under transient thermal conditions: A state-of-the-art review, Eng. Struct. 127 (2016) 172–188, https://doi.org/10.1016/j.engstruct.2016.08.021.
[54] U. Schneider, Concrete at High Temperatures – A General Review, Fire Saf. J. 13 (1988) 55–68, https://doi.org/10.1016/0379-7112(88)90033-1.
[55] Z.P. Bazant, Y. Xi, Drying creep of concrete: constitutive model and new experiments separating its mechanisms, Mater. Struct. 27 (1994) 3–14.
[56] S. Peters, G. Vu, G. Meschke, A multiscale model for predicting the Young's modulus and the thermal-expansion coefficient of concrete at high temperatures, Constr. Build. Mater. 479 (2025), https://doi.org/10.1016/j.conbuildmat.2025.141259.
[57] T. Koyama, M. Ozawa, M. Kanematsu, Study on the thermal shrinkage behavior of cement paste under high temperature envirnoment, Cem. Sci. Concr. Technol. 78 (2024) 128–136, https://doi.org/10.14250/cement.78.128.
[58] U. Schneider, Behav. Concr. High. Temp. Dtsch. Aussch. F. üR. Stahlbeton (1982) 1–110.